Computationally Efficient Nonlinear Edge Preserving Smoothing of n-D Medical Images Via Scale-Space Fingerprint Analysis[1]

BW Reutter,[†‡] *Member, IEEE*; VR Algazi,[‡] *Life Senior Member, IEEE*;
and RH Huesman,[†] *Senior Member, IEEE*
[†]Center for Functional Imaging, Lawrence Berkeley National Laboratory
University of California, Berkeley, CA 94720 USA
[‡]Center for Image Processing and Integrated Computing
University of California, Davis, CA 95616 USA

Abstract

Nonlinear edge preserving smoothing often is performed prior to medical image segmentation. The goal of the nonlinear smoothing is to improve the accuracy of the segmentation by preserving changes in image intensity at the boundaries of structures of interest, while smoothing random variations due to noise in the interiors of the structures. Methods include median filtering and morphology operations such as gray scale erosion and dilation, as well as spatially varying smoothing driven by local contrast measures.

Rather than irreversibly altering the image data prior to segmentation, the approach described here has the potential to unify nonlinear edge preserving smoothing with segmentation based on differential edge detection at multiple scales. The analysis of n-D image data is decomposed into independent 1-D problems that can be solved quickly. Smoothing in various directions along 1-D profiles through the n-D data is driven by a measure of local structure separation, rather than by a local contrast measure. Isolated edges are preserved independent of their contrast, given an adequate contrast to noise ratio.

I. Introduction

Nonlinear edge preserving smoothing often is performed prior to medical image segmentation. The goal of the nonlinear smoothing is to improve the accuracy of the segmentation by preserving changes in image intensity at the boundaries of structures of interest, while smoothing random variations due to noise in the interiors of the structures. Methods include median filtering and morphology operations such as gray scale erosion and dilation [1], as well as spatially varying smoothing driven by local contrast measures [2, 3]. By comparison, linear smoothing via spatially invariant convolution uniformly blurs structure boundaries, as well as noise. The benefits of noise reduction can be offset by deformations of the boundaries that adversely affect the accuracy of the subsequent segmentation.

Rather than irreversibly altering the image data prior to segmentation, the approach described here has the potential to unify nonlinear edge preserving smoothing with segmentation based on differential edge detection at multiple scales. The analysis of multidimensional (n-D) image data is decomposed into independent 1-D problems that can be solved quickly. Smoothing in various directions along 1-D profiles through the n-D data is driven by a measure of local structure separation, rather than by a local contrast measure. Isolated edges are preserved independent of their contrast, given an adequate contrast to noise ratio (CNR). In addition, analytic expressions are obtained for the derivatives of the edge preserved 1-D profiles. Using these expressions, one can compose multidimensional edge detection operators such as the Laplacian or the second derivative in the direction of the image intensity gradient.

Future applications of these methods include 4-D spatiotemporal segmentation of respiratory gated cardiac positron emission tomography (PET) transmission images to improve the accuracy of attenuation correction [4, 5], and 4-D spatiotemporal segmentation of dynamic cardiac single photon emission computed tomography (SPECT) images to facilitate unbiased estimation of time activity curves and kinetic parameters for left ventricular volumes of interest [6].

II. The 1-D Algorithm

A. Recursive Multiscale Blending

Given linearly smoothed versions of a 1-D signal $\mathrm{f}(x)$ and its first two derivatives at J scales, one can perform nonlinear edge preserving smoothing as follows. The linearly smoothed versions of $\mathrm{f}(x)$ are denoted by $\bar{\mathrm{f}}(x, a_j)$, and the linearly smoothed first and second derivatives are denoted by $\bar{\mathrm{f}}^{(1)}(x, a_j)$ and $\bar{\mathrm{f}}^{(2)}(x, a_j)$, respectively, for $j = 1, \ldots, J$. The scale coordinate a controls the width of the convolution kernels used in the linear filtering. The kernels are based on the uniform cubic B-spline basis function and its first two derivatives [7, 8]. The cubic B-spline has a support of $4a$ and approximates a Gaussian with a standard deviation, σ, of $\sqrt{1/3}\,a$. Dyadic sampling of the scale coordinate a is used, yielding $a_j = 2^{j-1}a_1$.

The nonlinearly smoothed versions of $\mathrm{f}(x)$, denoted by $\tilde{\mathrm{f}}(x, a_j)$, are obtained by recursively blending the linearly

[1]This work was supported by US Department of Health and Human Services grant P01-HL25840, by US Department of Energy contract DE-AC03-76SF00098, and by the University of California MICRO program. This work was developed in part using the resources at the US Department of Energy National Energy Research Scientific Computing (NERSC) Center.

smoothed versions:

$$\tilde{\mathrm{f}}(x,a_j) = \begin{cases} \bar{\mathrm{f}}(x,a_1) & j=1 \\ [1-\mathrm{C}_j(x)]\,\tilde{\mathrm{f}}(x,a_{j-1}) & \\ \quad +\mathrm{C}_j(x)\,\bar{\mathrm{f}}(x,a_j) & j=2,\ldots,J. \end{cases} \tag{1}$$

The blending functions $\{\mathrm{C}_j(x);\ j=2,\ldots,J\}$ play a role similar to that of the spatially varying diffusion coefficients used in typical implementations of edge preserving smoothing via inhomogeneous diffusion (e.g., [2]). When $\mathrm{C}_j(x_0)=0$, smoothing stops in the neighborhood of x_0 and $\tilde{\mathrm{f}}(x_0,a_j)$ remains unchanged from the value $\tilde{\mathrm{f}}(x_0,a_{j-1})$ obtained using nonlinear smoothing at the previous, finer scale. Conversely, when $\mathrm{C}_j(x_0)=1$, smoothing is unabated and $\tilde{\mathrm{f}}(x_0,a_j)$ is set to the value $\bar{\mathrm{f}}(x_0,a_j)$ obtained using linear smoothing at the current, coarser scale.

B. Defining the Blending Functions

The blending functions $\{\mathrm{C}_j(x);\ j=2,\ldots,J\}$ are defined via the following analysis of the augmented scale-space fingerprint for $\mathrm{f}(x)$. The augmented scale-space fingerprint (Figure 1) is a graphical depiction of the locations of the zero-crossings of the first two derivatives of the linearly smoothed signal as a function of scale [8]. At a particular scale a_j, each zero-crossing location of $\bar{\mathrm{f}}^{(2)}(x,a_j)$ is labeled as either a local maximum (edge) or local minimum (ledge) in gradient magnitude, depending on its proximity to nearby zero-crossing locations of $\bar{\mathrm{f}}^{(1)}(x,a_j)$ (i.e., ridges and troughs). For each of the resulting edge locations $\{x_{jk};\ k=1,\ldots,K_j\}$, the distance Δx_{jk} separating the ridge, trough, or ledge on either side of the edge is calculated. The blending function $\mathrm{C}_j(x)$ is then assigned values ranging between zero and one at the edge locations, based on the separation distances $\{\Delta x_{jk};\ k=1,\ldots,K_j\}$.

The value assigned to $\mathrm{C}_j(x)$ at the edge location x_{jk} is denoted by γ_{jk} and is selected using a monotonically decreasing function that maps larger separation distances to smaller values. This heuristic mapping is based on the observation that the separation distance Δx tends to be larger for an isolated true edge, than it is for a random second derivative zero-crossing associated with noise (Figure 1). For simplicity, a piecewise linear mapping is used:

$$\gamma_{jk} = \begin{cases} 1 & \Delta x_{jk} < \alpha_j \\ 1-\frac{\Delta x_{jk}-\alpha_j}{\beta_j-\alpha_j} & \alpha_j \le \Delta x_{jk} < \beta_j \\ 0 & \beta_j \le \Delta x_{jk}, \end{cases} \tag{2}$$

where α_j and β_j are selected as follows. The separation distances $\{\Delta x_{jk};\ k=1,\ldots,K_j\}$ are first sorted in ascending order, and then α_j and β_j are set to values corresponding to a lower and an upper percentile of the sorted values, respectively. The lower and upper percentiles can be selected based on the expected numbers of true and random edges at the j^{th} scale. In practice, the expected number of random edges due to noise in the linearly smoothed signal $\bar{\mathrm{f}}(x,a_j)$ will vary roughly inversely with the scale a_j, while the number of isolated true edges will remain roughly constant.

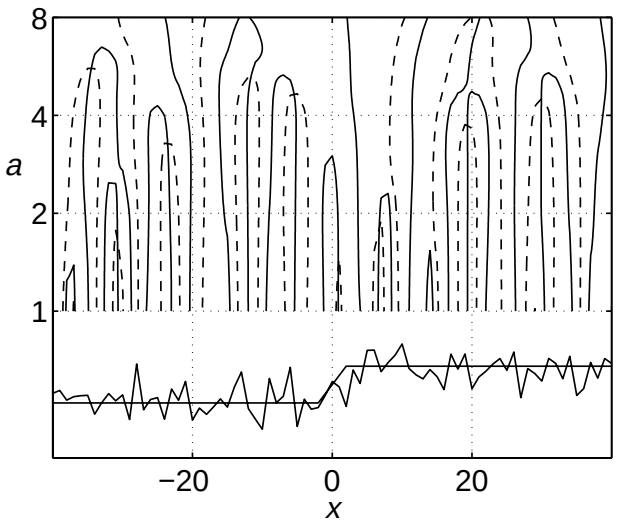

Figure 1: Augmented scale-space fingerprint for an isolated edge of width four and a CNR of 2.5. Solid fingerprint lines depict the zero-crossing locations of $\bar{\mathrm{f}}^{(2)}(x,a)$ (i.e., edge and ledge locations) over a continuum of scales. Dashed lines depict the zero-crossing locations of $\bar{\mathrm{f}}^{(1)}(x,a)$ (i.e., ridge and trough locations). The noiseless signal is shown with the noisy signal below the fingerprint.

Given the values $\{\gamma_{jk};\ k=1,\ldots,K_j\}$ at the edge locations, the blending function $\mathrm{C}_j(x)$ can be defined for all x as follows. The blending function $\mathrm{C}_j(x)$ must be continuous through at least its second derivative, in order for the nonlinearly smoothed signal $\tilde{\mathrm{f}}(x,a_j)$ to have continuous first and second derivatives. Rearranging the factors in equation (1) and denoting the first and second derivatives of $\mathrm{C}_j(x)$ by $\mathrm{C}_j^{(1)}(x)$ and $\mathrm{C}_j^{(2)}(x)$, respectively, one obtains the following expressions for the first and second derivatives of the nonlinearly smoothed signal $\tilde{\mathrm{f}}(x,a_j)$:

$$\tilde{\mathrm{f}}^{(1)}(x,a_j) = \begin{cases} \bar{\mathrm{f}}^{(1)}(x,a_1) & j=1 \\ \tilde{\mathrm{f}}^{(1)}(x,a_{j-1}) & \\ \quad +\mathrm{C}_j(x)\left[\bar{\mathrm{f}}^{(1)}(x,a_j)-\tilde{\mathrm{f}}^{(1)}(x,a_{j-1})\right] & j=2,\ldots,J \\ \quad +\mathrm{C}_j^{(1)}(x)\left[\bar{\mathrm{f}}(x,a_j)-\tilde{\mathrm{f}}(x,a_{j-1})\right] & \end{cases} \tag{3}$$

$$\tilde{\mathrm{f}}^{(2)}(x,a_j) = \begin{cases} \bar{\mathrm{f}}^{(2)}(x,a_1) & j=1 \\ \tilde{\mathrm{f}}^{(2)}(x,a_{j-1}) & \\ \quad +\mathrm{C}_j(x)\left[\bar{\mathrm{f}}^{(2)}(x,a_j)-\tilde{\mathrm{f}}^{(2)}(x,a_{j-1})\right] & \\ \quad +2\mathrm{C}_j^{(1)}(x)\left[\bar{\mathrm{f}}^{(1)}(x,a_j)-\tilde{\mathrm{f}}^{(1)}(x,a_{j-1})\right] & j=2,\ldots,J. \\ \quad +\mathrm{C}_j^{(2)}(x)\left[\bar{\mathrm{f}}(x,a_j)-\tilde{\mathrm{f}}(x,a_{j-1})\right] & \end{cases} \tag{4}$$

To achieve the desired continuity in a relatively straightforward fashion, the blending function $\mathrm{C}_j(x)$ is defined to be the

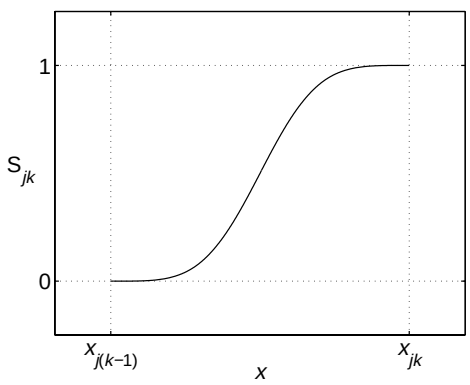

Figure 2: The smooth step function $\mathrm{S}_{jk}(x)$ given by equation (6).

piecewise quartic function

$$\mathrm{C}_j(x) = \begin{cases} \gamma_{j1} & x < x_{j1} \\ \gamma_{j(k-1)} + \left[\gamma_{jk} - \gamma_{j(k-1)}\right] \mathrm{S}_{jk}(x) & x_{j(k-1)} \le x < x_{jk}; \\ & k = 2, \ldots, K_j \\ \gamma_{jK_j} & x_{jK_j} \le x, \end{cases} \tag{5}$$

where $\mathrm{S}_{jk}(x)$ is a smooth step function obtained by integrating the uniform cubic B-spline basis function on which the linear smoothing is based:

$$\mathrm{S}_{jk}(x) = \int_{x_{j(k-1)}}^{x} \frac{1}{v_{jk}} \Pi^{*4}\left(\frac{u - u_{jk}}{v_{jk}}\right) du, \tag{6}$$

where $u_{jk} = \left[x_{j(k-1)} + x_{jk}\right]/2$, $v_{jk} = \left[x_{jk} - x_{j(k-1)}\right]/4$, and $\Pi^{*4}(u)$ denotes the uniform cubic B-spline basis function. The function $\mathrm{S}_{jk}(x)$ is zero at $x = x_{j(k-1)}$ and increases monotonically to one at $x = x_{jk}$ (Figure 2). It is continuous through its third derivative, and its first through third derivatives are all zero at both $x = x_{j(k-1)}$ and $x = x_{jk}$. Thus, using this construction one obtains a blending function $\mathrm{C}_j(x)$ that ranges between zero and one and is continuous through its third derivative.

III. The n-D Algorithm

Edges can be preserved in multidimensional image data by applying the 1-D algorithm independently along the coordinate axis directions, as well as along the diagonal directions of the 2-D planes spanned by the coordinate axes, and averaging the results. This builds on the work described in [2], in which processing was performed only along the coordinate axis directions.

By processing the diagonal directions, additional information is obtained that allows one to characterize the first and second order differential properties of the data in any direction [8]. Using this additional information, multidimensional edge detection operators such as the Laplacian or the second derivative in the direction of the gradient can be composed and used to segment the data [8].

IV. Results

A. Simulated 1-D Edge

To test the performance of the 1-D algorithm, Gaussian white noise was added to a simulated signal composed of a single ramp transition of width four and a CNR of 2.5 (Figure 1). Linear smoothing was performed at four scales using uniform cubic B-spline basis functions with scale parameters $a_1 = 1$, $a_2 = 2$, $a_3 = 4$, and $a_4 = 8$. Nonlinear smoothing was performed at the scales a_2, a_3, and a_4, using equation (1). Results at the scale a_4 are shown in Figure 3(a).

The blending functions $\mathrm{C}_2(x)$, $\mathrm{C}_3(x)$, and $\mathrm{C}_4(x)$ were defined using values for β_2, β_3, and β_4 in equation (2)

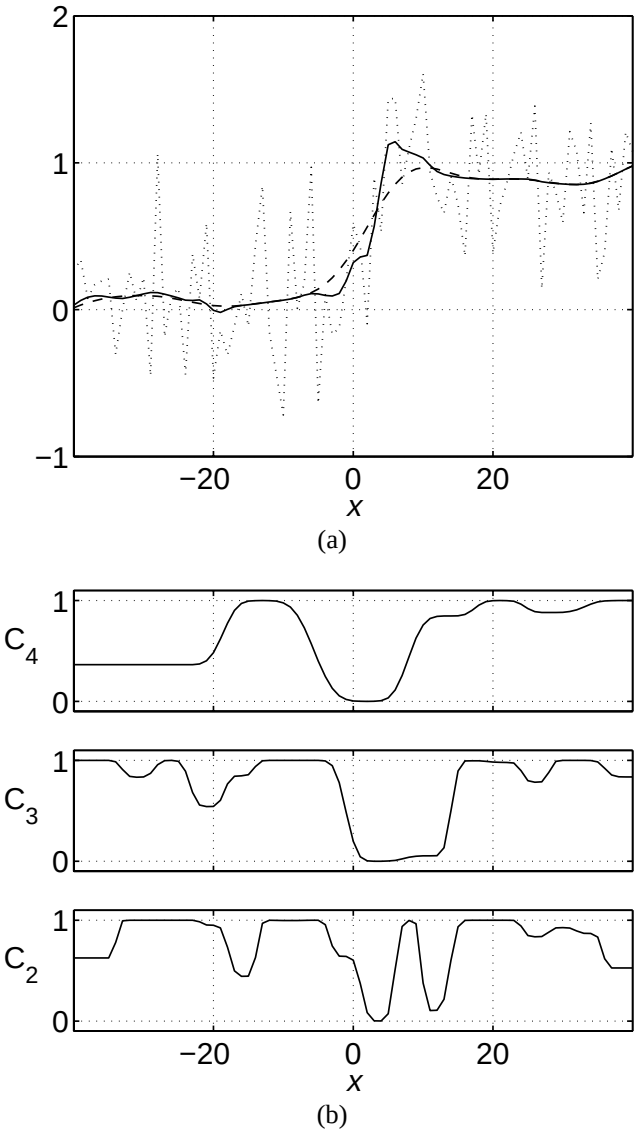

Figure 3: Results for a simulated 1-D edge of width four and a CNR of 2.5. In (a), the dashed line and the solid line depict the linear and nonlinear smoothing results, respectively, at the scale $a_4 = 8$. The dotted line depicts the unsmoothed signal, which is shown also in Figure 1 with its scale-space fingerprint. The blending functions used to perform the nonlinear smoothing are shown in (b).

corresponding to the 94^{th}, 89^{th}, and 80^{th} percentiles of the sorted separation distances, respectively [Figure 3(b)]. The upper percentile for β_4 was selected so that four out of every five edges would undergo some smoothing at the coarsest scale, $a_4 = 8$. Then, using the heuristic that the expected number of random edges due to noise varies roughly inversely with scale, the upper percentiles for β_3 and β_2 were selected so that eight out of nine edges and 16 out of 17 edges would undergo some smoothing at the finer scales $a_3 = 4$ and $a_2 = 2$, respectively. The lower percentiles associated with α_2, α_3, and α_4 in equation (2) were selected to be one-half of the upper percentiles, i.e., the 47^{th}, 44^{th}, and 40^{th} percentiles, respectively.

The nonlinear smoothing yielded a sharper edge than did the linear smoothing, and provided comparable smoothing away from the edge [Figure 3(a)]. The blending functions consistently reached their minimum near the edge, thus reducing the amount of smoothing in the neighborhood of the edge [Figure 3(b)]. Away from the edge, the blending functions increased, thus increasing the amount of smoothing.

B. Respiratory Gated PET Transmission Images

A 3-D version of the n-D algorithm was applied to respiratory gated PET transmission images analyzed previously in [5]. The images were reconstructed from 1.3 min of data (190,000 counts per transverse plane) acquired during the end-expiration respiratory phase [Figure 4(a)]. As a reference, Figure 4(b) shows results obtained using linear smoothing with a 7×7×7 operator that approximates a 3-D Gaussian.

The 1-D algorithm was applied independently along the x, y, and z coordinate axis directions of the 128×128×41 dataset, using the same linear filters that were used to process the simulated 1-D edge in Section IV.A. Six diagonal directions in the xy (transverse), xz (coronal), and yz (sagittal) planes were also processed. Figure 4(c) shows the results of simply averaging the outputs of the nine large scale (1×35) 1-D linear filters, corresponding to the scale parameter $a_4 = 8$. For independent, identically distributed Gaussian noise, this linear filtering operation would yield noise reduction comparable to that of the 7×7×7 operator used to obtain the results in Figure 4(b). For the case of these transmission images, averaging the outputs of the nine large scale 1-D linear filters appears to do a better job of decorrelating the noise, at the expense of blurring the edges.

Figure 4(d) shows the results of nonlinear smoothing at the scale $a_4 = 8$. The blending functions $\mathrm{C}_2(x)$, $\mathrm{C}_3(x)$, and $\mathrm{C}_4(x)$ were defined using values for β_2, β_3, and β_4 in equation (2) corresponding to the 80^{th}, 67^{th}, and 50^{th} percentiles of the sorted separation distances, respectively. The upper percentile for β_4 was selected so that one out of every two edges would undergo some smoothing at the coarsest scale, $a_4 = 8$. Then, using the heuristic that the expected number of random edges due to noise varies roughly inversely with scale, the upper percentiles for β_3 and β_2 were selected so that two out of three edges and four out of five edges would undergo some smoothing at the finer scales $a_3 = 4$ and $a_2 = 2$, respectively. The lower percentiles associated with α_2, α_3, and α_4 in equation (2) were selected to be one-half of the upper percentiles, i.e., the 40^{th}, 33^{rd}, and 25^{th} percentiles, respectively.

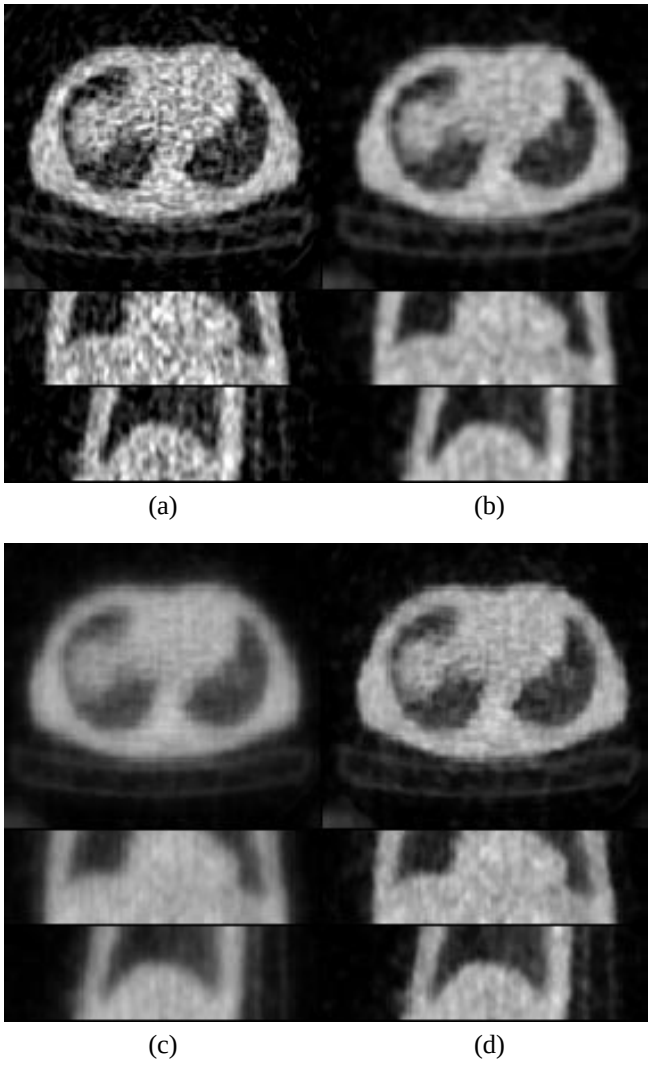

(a) (b)

(c) (d)

Figure 4: Results for respiratory gated PET transmission images. (a) Original images; (b) 7×7×7 linear smoothing; (c) average of large scale (1×35) 1-D linear smoothing operators applied along the three coordinate axis directions and six diagonal directions; and (d) large scale nonlinear smoothing. The top, middle, and bottom rows show transverse, coronal, and sagittal cross sections, respectively.

The nonlinear smoothing results shown in Figure 4(d) were obtained in only 9.3 min using a 195 MHz MIPS R10000-based Silicon Graphics workstation. These images are sharper and noisier than those shown in Figure 4(c). The nonlinear smoothing results appear to be sharper than, but not noisier than, the results shown in Figure 4(b).

V. Future Directions

Ultimately, the figure of merit for this methodology will be the accuracy of the segmentations obtained in conjunction with the nonlinear edge preserving smoothing, when applied to time sequences of noisy volumetric nuclear medicine images. We are working to implement the edge preserving

smoothing in 4-D, as well as to compose 4-D edge detection operators using the analytic expressions for the directional derivatives of the nonlinearly smoothed images. The University of North Carolina Mathematical Cardiac Torso (MCAT) phantom [9] will be used to validate the accuracy of the resulting spatiotemporal segmentations.

VI. Acknowledgment

This work was supported by the National Heart, Lung, and Blood Institute of the US Department of Health and Human Services under grant P01-HL25840; by the Director, Office of Science, Office of Biological and Environmental Research, Medical Sciences Division of the US Department of Energy under contract DE-AC03-76SF00098; and by the University of California MICRO program. This work was developed in part using the resources at the US Department of Energy National Energy Research Scientific Computing (NERSC) Center.

VII. References

[1] S R Sternberg, "Grayscale morphology," *Comput Vis Graph Imag Process*, vol. 35, no. 3, pp. 333–355, 1986.

[2] J Weickert, B M T H Romeny, and M A Viergever, "Efficient and reliable scheme for nonlinear diffusion filtering," *IEEE Trans Imag Process*, vol. 7, no. 3, pp. 398–410, 1998.

[3] K Kitamura, H Iida, M Shidahara, S Miura, and I Kanno, "Noise reduction in PET attenuation correction using non-linear Gaussian filters," *IEEE Trans Nucl Sci*, vol. 47, no. 3, pp. 994–999, 2000.

[4] B W Reutter, G J Klein, and R H Huesman, "Automated 3-D segmentation of respiratory-gated PET transmission images," *IEEE Trans Nucl Sci*, vol. 44, no. 6, pp. 2473–2476, 1997.

[5] B W Reutter, G J Klein, and R H Huesman, "Respiration-compensated cardiac PET attenuation correction via automated 4-D segmentation of gated transmission images," *J Nucl Med*, vol. 38, no. 5 suppl, pp. 203P, 1997, (abstract).

[6] B W Reutter, G T Gullberg, and R H Huesman, "Direct least-squares estimation of spatiotemporal distributions from dynamic SPECT projections using a spatial segmentation and temporal B-splines," *IEEE Trans Med Imag*, vol. 19, no. 5, pp. 434–450, 2000.

[7] Y-P Wang and S L Lee, "Scale-space derived from B-splines," *IEEE Trans Patt Anal Mach Intell*, vol. 20, no. 10, pp. 1040–1055, 1998.

[8] B W Reutter and V R Algazi, "Computationally efficient anisotropic scale-space processing of 4-D medical images," Tech. Rep. LBNL-42584, Lawrence Berkeley National Laboratory, 1998.

[9] W P Segars, D S Lalush, and B M W Tsui, "Modeling respiratory mechanics in the MCAT and spline-based MCAT phantoms," in *1999 IEEE Nuclear Science Symposium and Medical Imaging Conference Record*, J A Seibert, Ed., 2000, pp. 985–989.

Disclaimer